Molecular Calculation of the Critical Parameters of Classical Helium

Richard A. Messerly,[†,¶] Navneeth Gokul,[‡] Andrew J. Schultz,[‡] David A. Kofke,[‡] and Allan H. Harvey[*,†]

[†]*Applied Chemicals and Materials Division, National Institute of Standards and Technology, 325 Broadway, Boulder, CO 80305*

[‡]*Department of Chemical and Biological Engineering, University at Buffalo, The State University of New York, Buffalo, NY 14260-4200, USA*

[¶]*Present address: Biosciences Center, National Renewable Energy Laboratory, 15013 Denver W Pkwy, Golden, CO 80401*

E-mail: allan.harvey@nist.gov

Draft: June 18, 2019

Revision for *J. Chem. Eng. Data*

Abstract

We compute the vapor-liquid critical coordinates of a model of helium in which nuclear quantum effects are absent. We employ highly accurate *ab initio* pair and three-body potentials and calculate the critical parameters rigorously in two ways. First, we calculate the virial coefficients up to the seventh and find the point where an isotherm satisfies the critical conditions. Second, we use Gibbs Ensemble Monte Carlo (GEMC) to calculate the vapor-liquid equilibrium, and extrapolate the phase envelope to the critical point. Both methods yield results that are consistent within their uncertainties.

The critical temperature of "classical helium" is 13.0 K (compared to 5.2 K for real helium), the critical pressure is 0.93 MPa, and the critical density is 28.4 mol·L^{-1}, with expanded uncertainties (corresponding to a 95% confidence interval) on the order of 0.1 K, 0.02 MPa, and 0.5 mol·L^{-1}, respectively. The effect of three-body interactions on the location of the critical point is small (lowering the critical temperature by roughly 0.1 K), suggesting that we are justified in ignoring four-body and higher interactions in our calculations. This work is motivated by the use of corresponding-states models for mixtures containing helium (such as some natural gases) at higher temperatures where quantum effects are expected to be negligible; in these situations, the distortion of the critical properties by quantum effects causes problems for the corresponding-states treatment.

Keywords: critical parameters; Gibbs ensemble simulation; helium; nuclear quantum effects; thermodynamic properties; virial coefficients

Introduction

Helium is an important fluid in science and technology. Its primary terrestrial source is in certain natural gases, from which it is extracted. It is therefore necessary to include helium in thermophysical property models for natural gas. Unfortunately, helium is notoriously difficult to include in mixture equation-of-state (EOS) models or corresponding-states models. The reason is that these models combine the critical parameters for each pure component (typically the critical temperature, T_c, and critical pressure, P_c; sometimes the critical density ρ_c or the critical compressibility factor $Z_c \equiv \frac{P_c}{\rho_c R T_c}$ is also used, where R is the molar gas constant) to produce a thermodynamic surface for the mixture. For helium, the critical point is at such a low temperature (T_c is approximately 5.2 K) that it is significantly altered by quantum effects. These quantum effects largely vanish at the higher temperatures at which gas production and processing take place. Therefore, mixture models that use the measured critical parameters of helium tend to require extra adjustable parameters to make

up for this distortion.

This problem has led researchers to develop "effective" critical parameters that can be used for helium in mixture calculations. The first such attempt appears to be that of Newton.[1] The best-known approach in chemical engineering thermodynamics was developed by Prausnitz and coworkers,[2,3] who developed a set of temperature-dependent effective critical parameters for hydrogen, helium, and neon.

Recently, motivated by the inconvenience of temperature-dependent critical parameters for engineering calculations, Rowland et al.[4] developed a single set of effective critical constants for helium for use in calculations for natural gas mixtures. The new parameters (critical temperature $T_c = 11.73$ K, critical pressure $P_c = 0.568$ MPa) were obtained by examining mixture phase-equilibrium data for helium with methane, as modeled by the Peng-Robinson EOS, and were shown to improve Peng-Robinson predictions for other helium-containing mixtures. It is not yet clear whether these effective parameters are useful only in the context of the Peng-Robinson equation, or whether they might also be useful for other approaches such as the GERG-2008 EOS[5] that is commonly used for natural gas. The possible dependence of the effective critical parameters on the EOS used may limit the applicability of the approach of Rowland et al.[4]

We take a complementary approach to this problem by determining from molecular properties what the critical parameters would be for hypothetical "classical" helium. While in the past such an approach would have had to rely on empirical mapping of experimental data for helium onto a non-quantum fluid such as argon (which is approximately what Gunn et al.[2] did over 50 years ago), today the development of highly accurate two-body[6] and three-body[7] intermolecular potentials for helium allows more rigorous calculation of the classical critical point.

In this work, we will examine three approaches to calculating the critical constants of classical helium from the intermolecular forces. First, we will briefly examine simple methods based only on the pair potential. Second, we will use rigorous calculations of the virial

coefficients, including three-body contributions but not nuclear quantum effects, to estimate the critical point. Third, we will estimate the critical point from molecular simulation of the phase equilibria using Gibbs Ensemble Monte Carlo (GEMC). In addition, we will perform the virial and the molecular simulation calculations for the case where only two-body interactions are considered; this will tell us the relative importance of the three-body interactions. If the effect of the three-body interactions is small, this will provide justification for ignoring four-body and higher effects.

Potentials

Przybytek et al.[6] recently reported a state-of-the-art pair potential for helium that improves on the already excellent potential of Cencek et al.[8,9] It incorporates highly accurate results not only for the potential energy in the Born-Oppenheimer (BO) approximation, but also for the most important post-BO effects (adiabatic, relativistic, and quantum electrodynamics). The potential of Cencek et al. was used to obtain values for the second virial coefficient $B_2(T)$ and for the low-density limits of the viscosity and thermal conductivity with much smaller uncertainty than any existing experiment.[9]

However, pair potentials alone cannot quantitatively describe real fluids except at low densities. For condensed phases, often even the addition of three-body forces is not enough for quantitative accuracy; for example, Schwerdtfeger et al. showed that four-body forces were required for accurate description of solid argon.[10] However, for smaller, less polarizable species, there is reason to think that three-body forces are sufficient. Schwerdtfeger and Hermann showed that two-and three-body forces could describe solid neon.[11] For helium, three-body energies are on the order of a percent or less of the two-body contributions[7] and make only a small (on the order of 1%) contribution to the third virial coefficient $B_3(T)$,[12] suggesting that the multibody expansion converges quickly and that four-body and higher energies will be negligible. We use the three-body potential developed at the full-

configuration-interaction (FCI) level by Cencek et al.[7] The uncertainty of the three-body potential, which accounts for nonadditivity in both the attractive and repulsive forces, is estimated by the authors to be 2%.

The uncertainties reported herein are only numerical uncertainties associated with the virial calculations and molecular simulations themselves,[13] i.e., they do not account for the uncertainties in the underlying two- or three-body potentials. Because of the extremely small uncertainty of the pair potential,[6] we expect the uncertainties in the virial coefficients to be dominated by the uncertainty in the three-body potential. By contrast, the uncertainties that arise from the two- and three-body potentials are likely negligible compared with the relatively large GEMC statistical uncertainties and uncertainties associated with extrapolation to the critical point.

Calculations Based on the Pair Potential

Before we turn to more rigorous calculations of the critical properties based on the pair and three-body potentials, we examine three simpler methods that use only the pair potential. Because of the small magnitude of multibody forces in helium, it is plausible that simple pair-based calculations will produce reasonable results. Perhaps the simplest approach is to map helium onto the well-known Lennard-Jones (LJ) model. In their thorough study of the LJ fluid critical properties, Dinpajooh et al.[14] reported reduced critical parameters $T_c^* \equiv T_c k_B/\epsilon = 1.3128(16)$, $P_c^* \equiv P_c\sigma^3/\epsilon = 0.1274(13)$, and $\rho_c^* \equiv \rho_c\sigma^3 = 0.316(4)$ (quoting $k = 2$ expanded uncertainties), where ϵ and σ are the LJ energy and size parameters, respectively, and k_B is the Boltzmann constant. For the effective LJ parameters of helium, we adopt the values from a recent evaluation by Weaver and Alexeenko:[15] $\epsilon/k_B = 9.8725$ K and $\sigma = 0.25238$ nm. This produces $T_c = 12.96$ K, $P_c = 1.08$ MPa, and $\rho_c = 32.4$ mol·L^{-1}.

A second approach involves matching the classical second virial coefficient $B_2(T)$ to that of a "simple" fluid (acentric factor $\omega = 0$) in the widely used Pitzer acentric factor system.

The function $B_2(T)$ for such fluids was described by Tsonopoulos.[16] A convenient way to estimate the critical temperature is given by the Boyle temperature where B_2 crosses zero; this is at a reduced temperature T/T_c of approximately 2.7 in the Tsonopoulos correlation. The high-accuracy pair potential of Przybytek et al.[6] produces a classical Boyle temperature just below 34 K, resulting in $T_c = 12.75$ K. The critical pressure can then be estimated by adjusting P_c until the $B_2(T)$ function of Tsonopoulos matches that calculated from the pair potential. This is somewhat subjective since the curves do not have exactly the same shape; we estimated $P_c = 0.94$ MPa.

Finally, we can employ the approach of Song and Mason,[17] who used an EOS they had successfully developed for nonpolar fluids[18] that requires only the pair potential. They used an early, less accurate helium potential,[19] and unfortunately they did not report the critical parameters for their EOS. We therefore repeated their calculations with the potential of Przybytek et al.[6] To find the critical point, we calculated isotherms $P(\rho)$ and found the isotherm that had a horizontal inflection point. The resulting critical point is $T_c = 13.05$ K and $P_c = 0.91$ MPa.

All three methods based on the pair potential give relatively consistent results, with critical temperatures between 12.75 K and 13.05 K and critical pressures between 0.91 MPa and 1.08 MPa. These rough estimates provide a range of expected values for the more rigorous methods that are presented in the following sections.

Calculation from Virial Expansion

Virial coefficients

The virial equation of state[20] expresses the pressure as a power series in the molar density:

$$\frac{P}{k_B T} = \rho + B_2(T)\rho^2 + B_3(T)\rho^3 + \dots \tag{1}$$

The coefficients B_n are the virial coefficients and depend only on temperature. In practice the series is truncated at order n (that is, retains terms up to and including $B_n\rho^n$), and we designate the n^{th}-order virial equation of state as VEOSn. The virial coefficients can be expressed rigorously for a given molecular model in terms of a so-called cluster integral, which we write generally as:

$$B_n = \frac{1-n}{n!} \int f_B\left(\mathbf{r}^n\right) \mathrm{d}\mathbf{r}^{n-1} \tag{2}$$

Here, f_B is a function of the configuration of the n atoms, as indicated by $\mathbf{r}^n$, and the integral is performed over the coordinates of $n-1$ of them, while one atom defines the origin in an otherwise infinite volume. The f_B function is often expressed as a sum of biconnected graphs with bonds representing the Mayer f-function; however, this formulation applies only to pairwise additive potentials and a more general expression is needed when multibody interactions are relevant, such as the present case. Regardless, f_B can be computed using the algorithm of Wheatley,[21] because it applies also to multibody potentials.[22] Normally, one must apply corrections to Eq. (2) to capture nuclear quantum effects. At not-too-low temperatures, this can be done using a semi-classical approximation,[23] but at the low temperatures of interest to the critical point, path-integral methods are needed. Coefficients B_n have been computed this way and reported for $n = 2-5$,[12,24–26] but of course the present study explicitly excludes quantum effects, so path-integral calculations were not performed in this work.

The coefficient B_2 and the additive component of B_3 were computed according to Eq. (2), using quadrature and Fourier transforms respectively, for the pair potential specified by Przybytek et al.[6] These coefficients were evaluated at temperatures from 10 K to 16 K in steps of 0.1 K with a tolerance of 10^{-8} (Å^3/molecule)$^{n-1}$, where 1 Å $\equiv 10^{-10}$ m. They were then fit using a polynomial in $\beta \equiv 1/k_{\text{B}}T$.

All other coefficients—that is, all coefficients excluding B_2 and the additive component of

B_3—were evaluated via Mayer sampling Monte Carlo (MSMC)[27] with overlap sampling.[28,29] The integrand in Eq. (2) was computed by employing the recursion developed by Wheatley.[21] This recursion enables the evaluation of the temperature derivatives of the virial coefficients on-the-fly for almost no added computational cost.[22]

In an attempt to improve the efficiency of the calculations, the reported values for B_4 to B_7 were computed in stages. As mentioned above, the targeted coefficient B_n is based on the 2017 pair potential of Przybytek et al.[6] with three-body interactions given according to Cencek et al.;[7] here we denote this coefficient using the notation $B_n[\mathrm{e},3]$. Rather than compute this directly, we first compute the coefficient $B_n[\mathrm{c},2]$, which does not include the three-body potential, and which describes pair interactions not with the computationally expensive (denoted e) 2017 potential,[6] but using the computationally cheap (denoted c) potential previously given in 2010 by Przybytek et al.[8] with more detail provided by Cencek et al.[9] From this starting point, we arrive at $B_n[\mathrm{e},3]$ by adding results from three more cluster-integral calculations:

$$B_n[\mathrm{e},3] = B_n[\mathrm{c},2] + \Delta B_n^{\mathrm{a}} + \Delta B_n^{\mathrm{b}} + \Delta B_n^{\mathrm{c}} \tag{3a}$$

where the differences are defined as follows. First:

$$\Delta B_n^{\mathrm{a}} = B_n[\mathrm{e},2] - B_n[\mathrm{c},2] \tag{3b}$$

This quantity is for coefficients based on only the pair potentials, differencing the computationally expensive and cheap versions. Second:

$$\Delta B_n^{\mathrm{b}} = B_n[\mathrm{c},3] - B_n[\mathrm{c},2] \tag{3c}$$

This is the contribution of the non-additive potential[7] to the virial coefficient, based on the

cheap[8,9] pairwise model. Finally,

$$\Delta B_n^{\mathrm{c}} = \{B_n[\mathrm{e},3] - B_n[\mathrm{e},2]\} - \{B_n[\mathrm{c},3] - B_n[\mathrm{c},2]\} \tag{3d}$$

This is the non-additive contribution differenced between the computationally expensive and cheap pair models. The advantage of computing the coefficient $B_n[\mathrm{e},3]$ this way instead of directly is that each of the terms given by Eqs. (3b), (3c), and (3d) is relatively small, so they can each be computed with less sampling to achieve a given precision. Each term is evaluated in a single MSMC calculation according to Eq. (2), but with an integrand that is the respective difference in f_B functions. In practice, we find that building up to the expensive 2017 pair potential from the cheap 2010 version has limited value for this application—for B_4 the computational savings are about a factor of 2, while for B_7 the approach does not provide any improvement in efficiency. This is because the largest part of the calculation time is spent on the Wheatley recursion, which is performed on a configuration after the potential function has been used.

Calculations were run at 10 K, 13 K, and 16 K and yielded the coefficient along with its first three temperature derivatives. The differences ΔB_n^{a} and ΔB_n^{c} were run for 10^6 steps and are very precise. The coefficients $B_n[\mathrm{c},2]$ were run for 10^{10} steps for $n = 4$, 10^9 steps for $n = 5$ and 6, and 10^8 steps for $n = 7$, while ΔB_n^{b} were run for 10^9 steps for $n = 3$ and 4, and 10^8 steps for $n = 5$, 6, and 7. Both $B_n[\mathrm{c},2]$ and ΔB_n^{b} were found to be given with significantly less precision than ΔB_n^{a} and ΔB_n^{c}, so additional sampling was performed, allocating effort in amounts that depend on the ratios of their respective difficulties ($D \equiv ut^{1/2}$, where u is the uncertainty obtained with computational effort t).[30] All contributions to $B_n[\mathrm{e},3]$ were combined according to Eq. (3) and fit using a polynomial in $Y \equiv \exp(a/k_{\mathrm{B}}T) - 1$, where a is a fitting parameter (along with the polynomial coefficients). Uncertainties in the fits have been obtained by bootstrapping, based on uncertainties in the virial coefficients (which themselves are obtained as the standard deviation of the mean of uncorrelated block averages). All virial

coefficient values and fitting coefficients are recorded in the Supporting Information.

Critical properties

The VEOS can be applied to estimate the critical point by searching for the temperature and density where Eq. (1) exhibits a positive horizontal inflection point, i.e., $\mathrm{d}P/\mathrm{d}\rho = \mathrm{d}^2P/\mathrm{d}\rho^2 = 0$ and $\mathrm{d}^3P/\mathrm{d}\rho^3 > 0$ at T_c, ρ_c. One can do this for increasing order of the series, i.e., using equation of state VEOSn, and observe whether the estimates of the critical properties appear to converge. We found[31,32] that for the LJ potential, this approach yields values of T_c and P_c that are in very good agreement with molecular simulation; effective convergence appears to occur at $n = 6$ (see Fig. 1). However, the critical density given this way is systematically too small. It is likely that this is a consequence of the singular nature of the critical point, which cannot be described using an analytical EOS. The critical isotherm approaches the critical density as $P \sim P_\mathrm{c} + A\,(\rho_\mathrm{c} - \rho)^\delta$, where the critical exponent δ is approximately 4.8.[33,34] As a remedy, we formulated in Reference 35 an approximant that captures the non-analytic approach to the critical point while providing behavior consistent with the virial series at low density.[35] The critical density can be computed for a given T_c and P_c using the approximant, and in application to the LJ model we obtained[35] a value for ρ_c this way that is consistent with the best estimates based on molecular simulation.

Critical properties determined from VEOSn, $n = 3$ to 7, are presented in Table 1. The table includes values of the critical density both from the inflection-point calculation and from the approximant; all approximant values of ρ_c use T_c and P_c as given by VEOS6. As shown in Fig. 1, the critical temperature appears to be converging with increasing series order, approaching a value between about 13.0 K and 13.5 K. The effect of including B_7 is to add more noise than to improve convergence—the coefficient is going through zero in the close vicinity of T_c, so it is difficult to determine a value that is as precise as its effect on T_c. In retrospect, we might have obtained a more useful result by evaluating the coefficient within a narrower range about the estimated T_c.

Additionally, in Table 1 and Fig. 1 we include calculations of the critical properties for the helium model using only the pairwise-additive contribution, omitting the three-body potential. We see that the effect of the non-pairwise contributions is to lower T_c by about 0.1 K, suggesting that the three-body potential is effectively repulsive at these temperatures. This is consistent with the finding of Garberoglio and Harvey[12] that the three-body contribution to B_3 is positive below approximately 170 K.

Extrapolation to $n \to \infty$

The oscillatory form of the critical properties with $1/n$ makes it difficult to extrapolate to $1/n \to 0$ in a methodical or precise way. However, the similarity of the helium behavior to that exhibited by the LJ model suggests that we can leverage the known behavior of the LJ model[32,36,37] to aid with the extrapolation of the helium VEOS results. In particular, if we assume that $T_c^{He}(n)/T_c^{LJ}(n)$ (where the n argument indicates the property computed using VEOSn) has regular behavior with $1/n$, we can extrapolate this ratio to $1/n \to 0$ and multiply by the critical temperature of LJ known from molecular simulation[38,39] (designated T_c^{LJ}(Sim)) to estimate the helium critical temperature. This is demonstrated in Fig. 1, with the result included in Table 1.

We are wary of extrapolating a quantity that we do not know to have a particular behavior in the limit of $n \to \infty$, and more specifically we do not feel justified in applying an extrapolation any more complicated than a linear form. A χ^2 analysis indicates that a linear fit that includes $n = 3$ does not match the values to within their uncertainties, so we omit the $n = 3$ point from the fit. The $n = 6$ and $n = 7$ values do not fit particularly well, but they have larger uncertainties, and a bootstrap analysis indicates that they have significant correlation with each other (see Supporting Information). When these factors are considered, the data for $n = 4$ to 7 can (barely, $p = 0.02$) be described via a straight-line fit, which we extrapolate to estimate the critical temperature for $1/n \to 0$.

The Supporting Information includes corresponding plots for the critical pressure and

density, along with other details of the analysis. The extrapolated values are included in Table 1. We find that T_c based on the two-body potential alone cannot be similarly fit within uncertainties by a straight line, so we do not report $1/n \to 0$ extrapolated properties for this case.

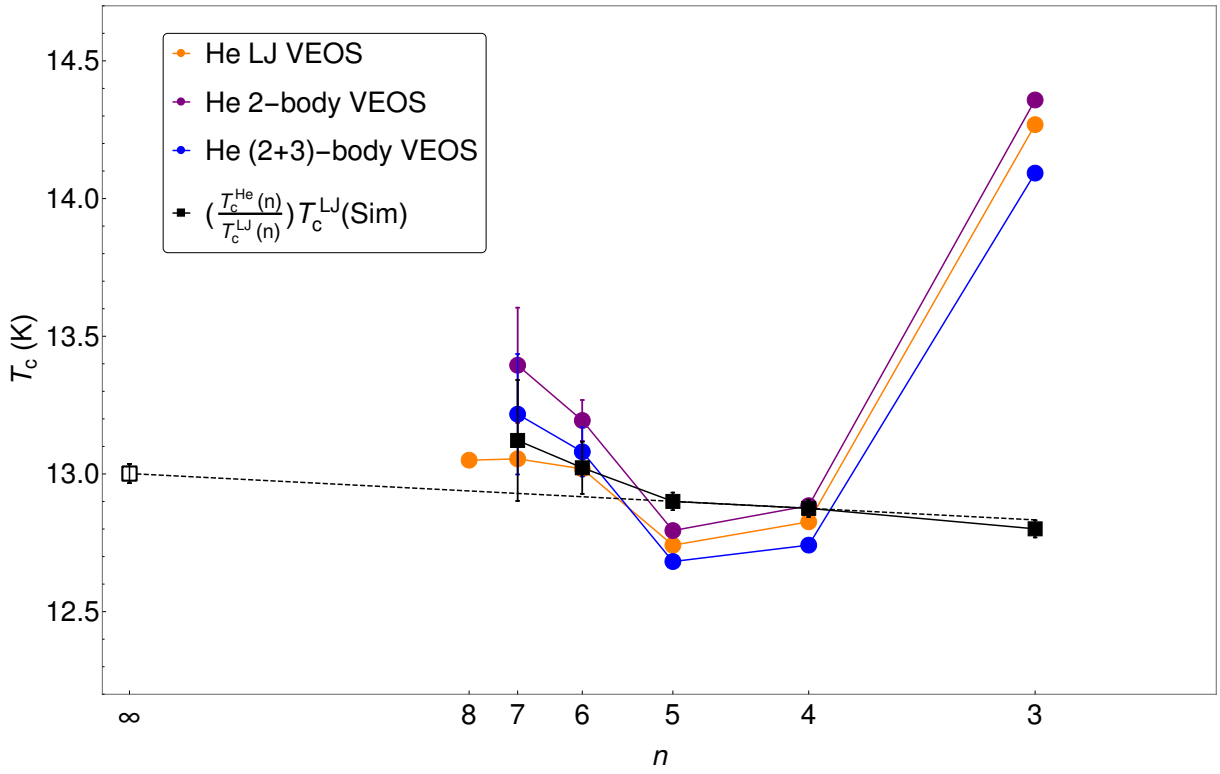

Figure 1: Critical temperature as given by the VEOSn as a function of series order n (presented against $1/n$, so the converged value would be represented by the y-intercept). Values are shown for the classical helium model (up to $n = 7$) both with and without the three-body potential, and for the Lennard-Jones (LJ) model (up to $n = 8$), using virial coefficients reported in previous work,[32] and using LJ size and energy parameters[15] $\epsilon/k_B = 9.8725$ K and $\sigma = 0.25238$ nm. The dashed line is a linear fit of the black squares (excluding $n = 3$), which is the LJ-assisted extrapolation construct described in the text; the $n \to \infty$ extrapolated value is shown by the open black square. Error bars represent 95% confidence intervals, which are approximately equivalent to an expanded uncertainty with coverage factor $k = 2$.

Table 1: Critical properties based on virial coefficients to the indicated order n. ρ_c^a is based on a critical isotherm approximant using T_c and P_c as given here for $n = 6$. The $n = \infty$ predictions for T_c, P_c and ρ_c are based on Lennard-Jonesian extrapolation as described in the text. Numbers in parentheses indicate the expanded uncertainty (95% confidence) in the last digit(s) of the tabulated value; these errors are propagated from the stochastic uncertainty in the virial coefficients, and do not include any effects of inaccuracy in the two- and three-body potentials.

	(2+3)-body				two-body			
n	T_c / K	P_c / MPa	ρ_c / mol·L^{-1}	ρ_c^a / mol·L^{-1}	T_c / K	P_c / MPa	ρ_c / mol·L^{-1}	ρ_c^a / mol·L^{-1}
3	14.09240(8)	1.23325(2)	31.5758(4)	33(1)	14.36(0)	1.30(0)	32.78(0)	33(1)
4	12.7416(4)	0.86147(10)	23.142(2)	32(2)	12.8847(4)	0.88633(10)	23.476(2)	32(1)
5	12.682(6)	0.8464(16)	22.73(4)	31(2)	12.794(6)	0.8632(15)	22.86(4)	31(1)
6	13.08(9)	0.97(3)	28(6)	31(2)	13.19(7)	0.98(3)	28(4)	31(1)
7	13.2(2)	1.02(8)	29(3)	30(2)	13.4(2)	1.06(7)	29(2)	30(2)
∞	13.00(4)	0.928(13)	28.3(4)	-	-	-	-	-

Calculation from Gibbs Ensemble Simulation

Simulation methods

Gibbs Ensemble Monte Carlo (GEMC) is a common, fast, and simple molecular simulation approach for computing vapor-liquid phase equilibria with a given potential.[40] We perform GEMC simulations at reduced temperatures ($T_r \equiv T/T_c$) between approximately 0.7 and 0.95. These subcritical simulation results are subsequently extrapolated to the critical point, as described in the next section. A summary of the GEMC simulation specifications is provided in Table 2.

Table 2: Gibbs Ensemble Monte Carlo simulation specifications.

Number of molecules, N	800, 1400, 2800
Temperature, T (K)	9.0 to 12.5 ($\Delta T = 0.5$)
Long-range cut-off distance, r_{cut} (nm)	1.0, 1.4, 1.8
Short-range cut-off distance, r_{inter} (nm)	0.15
Number of replicates, N_{reps}	4
Pre-equilibration Monte Carlo steps, MCS_{pre}	1×10^5
Equilibration Monte Carlo steps, MCS_{eq}	3×10^7
Production Monte Carlo steps, MCS_{prod}	1×10^8
Probability of translation move, Pr_{trans}	0.877
Probability of volume move, Pr_{vol}	0.003
Probability of swap move, Pr_{swap}	0.12

GEMC simulations couple two simulation boxes that correspond to the vapor and liquid phases. Three types of Monte Carlo moves are required to perform GEMC simulations of a single-site molecule that lacks rotational and torsional degrees of freedom, such as helium. Translation, volume, and particle swap Monte Carlo moves ensure thermal, pressure, and chemical equilibrium between the two phases, respectively. Translation moves displace one of the N particles (helium atoms) in a random direction by a random fraction of the prescribed maximum displacement. Volume moves exchange volume between the two boxes, where the magnitude of the volume exchange is a random fraction of the prescribed maximum volume change. Particle swap moves randomly delete a particle from one of the two boxes (chosen at random) and insert that particle into the other box at a random position.

All simulations are performed utilizing a customized form of the Cassandra v1.2 open-source parallelized Monte Carlo package.[41] Extension of the Cassandra code was necessary to implement the two- and three-body potentials. This was accomplished by first converting the Fortran77 code (available in References 7 and 8) for computing energies and forces into Fortran90 modules compatible with Cassandra. Furthermore, because the native Cassandra code stores an $N \times N$ pair-interactions matrix to avoid recomputing all interactions for translation and swap moves, our three-body extension of Cassandra stores an $N \times N \times N$ triplet-interactions matrix.

Simulations are divided into three stages. First, the liquid and vapor boxes are treated independently as de-coupled NVT (constant number of molecules, volume, and temperature) systems. Only translation moves are proposed during this pre-equilibration stage. This is followed by an equilibration stage, where all three types of moves are proposed, but the size of the maximum translation displacement and the maximum volume exchange is adjusted to meet a predetermined target acceptance rate of 50% (as prescribed by the native Cassandra code). This is followed by the production stage, where the sizes of the maximum translation displacement and maximum volume exchange are held constant. The number of Monte Carlo steps (MCS) for the pre-equilibration, equilibration, and production stages are recorded in

Table 2.

The probabilities (Pr) used during the equilibration and production stages for attempting a translation, volume, and particle swap Monte Carlo move are also given in Table 2. The low probability for attempting expensive volume moves is especially important for the simulations that include three-body effects, because volume moves require that the positions of all particles be scaled and the energies recomputed "from scratch." However, our $\mathrm{Pr}_{\mathrm{vol}}$ value is still consistent with the state-of-the-art GEMC protocol of 1 accepted volume move per N Monte Carlo moves (for $N = 800$).[42]

Four replicate simulations ($N_{\mathrm{reps}} = 4$) are performed at each temperature. To ensure independence between replicates, the entire sequence of pre-equilibration, equilibration, and production stages is repeated for each replicate. Replicate simulations are obtained by utilizing different random seeds for the initial configuration, move proposals, and move acceptance.

The initial simulation box configurations are constructed using Cassandra's internal initialization function. The initial densities for the liquid and vapor boxes are obtained from previous exploratory GEMC simulations. The initial numbers of molecules in each box are such that between 10% and 20% are in the vapor box, consistent with recent GEMC recommended practice.[14,42]

Analytic long-range tail corrections are included for the two-body potential for both energy and pressure, while long-range three-body interactions are neglected. Both the two- and three-body potentials utilize the same cut-off distance (r_{cut}). A three-body interaction is considered to be within the cut-off only when each atom of the triad is within r_{cut} of the other two atoms, i.e., $r_{ij} < r_{\mathrm{cut}}$, $r_{ik} < r_{\mathrm{cut}}$, and $r_{jk} < r_{\mathrm{cut}}$. For computational reasons, the three-body simulations only utilize the shorter cut-off distance of 1.0 nm.

An internal cut-off (r_{inter}) of 0.15 nm is also employed to improve computational efficiency by automatically rejecting any move that results in near overlap between two atoms, i.e., a proposed MC move is rejected when any pair distance is less than r_{inter}. Each attempted particle swap move considers 12 independent target locations in parallel, where a relatively

short long-range cut-off is utilized (r_{cut} = 0.65 nm) when computing the corresponding Rosenbluth weights.

To reduce computational time, three-body forces are not included in the virial pressure calculation. This simplification does not affect the vapor-liquid coexistence densities, because the GEMC acceptance criteria for translation, volume, and particle swap moves do not depend on pressure. Previous studies suggest that three-body repulsive and dispersive terms essentially cancel out in the vapor phase, such that excluding three-body forces should not significantly affect the vapor pressure calculations either.[43,44] We verified this by using VEOS6 (with three-body terms included in calculating the virial coefficients) to independently calculate the pressure at the GEMC coexisting vapor densities; the differences were much smaller than the uncertainty of the simulations (see Supporting Information). Therefore, any discrepancies between the two-body and (2+3)-body P^{sat} values should instead be attributed to differences in the vapor densities.

Reference 14 demonstrates that finite-size effects are negligible for GEMC simulations of the Lennard-Jones fluid at near-critical conditions for systems of 800 particles and $r_{\text{cut}} = 3.5\sigma$. To verify that their findings apply to our system of interest, we also perform GEMC simulations with 800, 1400, and 2800 helium atoms and r_{cut} = 1 nm, r_{cut} = 1.4 nm, and r_{cut} = 1.8 nm. These distances correspond to approximately 4σ, 5.5σ, and 7σ, where σ is the distance at which the helium two-body energy is zero ($\sigma \approx 0.26$ nm). Because the helium two-body potential decays to zero at a faster rate than the Lennard-Jones potential, the magnitude of the long-range contribution to energy and pressure is even less than that of the LJ potential for the same reduced cut-off distance.

Note that the GEMC simulations of the Lennard-Jones fluid performed in Reference 14 utilized larger system sizes (e.g., 5500), longer cut-offs (e.g., 8σ), and longer simulations (e.g., equilibration and production periods of 8.8×10^8 and 5.3×10^9 MCS, respectively) than those specified here. The primary reason for this difference is that the two- and three-body potentials utilized in the present study are significantly more expensive than the Lennard-

Jones potential. Furthermore, Reference 14 focuses on simulations at temperatures between $0.95T_c$ and T_c. By limiting our study to subcritical state points, finite-size effects are less significant and longer simulations are unnecessary.

To validate the two-body results obtained with the modified Cassandra code, additional two-body simulations are also performed with the native tabulated potential in the Towhee MCCCS code version 7.2.0.[45] Results obtained with Cassandra and Towhee are statistically indistinguishable (see Supporting Information). The Cassandra and Towhee simulations utilize the L'Ecuyer[46] and DX-1597-2-7[47] pseudo-random number generators, respectively. All necessary files to replicate the Cassandra simulations are provided as Supporting Information and at https://github.com/ramess101/Helium_ab_initio.

Post-simulation analysis

The critical temperature and critical density are obtained indirectly from GEMC results by simultaneously fitting the saturated liquid densities ($\rho_{\text{liq}}^{\text{sat}}$) and saturated vapor densities ($\rho_{\text{vap}}^{\text{sat}}$) to the law of rectilinear diameters and density scaling law:[48,49]

$$\rho_r \equiv \frac{\rho_{\text{liq}}^{\text{sat}} + \rho_{\text{vap}}^{\text{sat}}}{2} = \rho_c + A(T_c - T) \tag{4}$$

$$\rho_s \equiv \rho_{\text{liq}}^{\text{sat}} - \rho_{\text{vap}}^{\text{sat}} = B(T_c - T)^{\beta} \tag{5}$$

where ρ_r is the rectilinear diameters density, ρ_s is the scaling density, ρ_c, T_c, A, and B are fitting parameters, and β is assigned to a constant value of 0.355, which is a typical "effective" critical exponent when covering a wider range than the immediate critical region.[50]

The critical pressure is obtained by fitting the GEMC saturated vapor pressures (P^{sat}) to the Antoine equation[48]

$$\log_{10}\left(\frac{P^{\text{sat}}}{1\text{ MPa}}\right) = a_0 + \frac{a_1}{a_2 + T^{\text{sat}}} \tag{6}$$

where a_i are fitting constants, a_1 and a_2 have units of K, and a_1 is constrained to be negative. P_c is equal to P^{sat} in Eq. 6 evaluated at $T^{sat} = T_c$ with the optimal values of a_i.

Because the uncertainties in ρ_{liq}^{sat}, ρ_{vap}^{sat}, and P^{sat} increase near the critical point, Eqs. 4, 5, and 6 are fit using a weighted least-squares regression, where the weights are set equal to the inverse variance for ρ_r, ρ_s, and $\log_{10}\left(\frac{P^{sat}}{1\text{ MPa}}\right)$, respectively. The variance (equal to the square of the standard deviation) can be computed using several different methods, e.g., block averaging or replicates. Due to the low number of replicates (4) utilized in this study, we instead compute the variances using correlations found in Reference 51 for the standard deviation of ρ_r, ρ_s, and ρ_{vap}^{sat}. Note that, by assuming an ideal gas (linear) relationship between P^{sat} and ρ_{vap}^{sat}, the standard deviation for $\log_{10}\left(\frac{P^{sat}}{1\text{ MPa}}\right)$ is calculated as the standard deviation of ρ_{vap}^{sat} multiplied by $\frac{\log_{10}(e)}{\rho_{vap}^{sat}}$. As Eqs. 4, 5, and 6 are most reliable in the near-critical region, only GEMC results for $T_r \geq 0.75$ (i.e., $T \geq 10$ K) are included in the fitting procedure.

The uncertainties in the critical constants are obtained with bootstrap resampling. Specifically, Eqs. 4, 5, and 6 are refit thousands of times to random subsets of the GEMC simulation data. In addition, to account for the uncertainty in the scaling parameter β, each fit utilizes a different random value of β selected from a uniform distribution between 0.325 and 0.385. The 95% confidence intervals are estimated from the bootstrapped distribution of critical constant values. Recall that these uncertainties do not reflect the uncertainties in the two- or three-body potentials, which are assumed to be negligible compared to the GEMC numerical uncertainties.

GEMC simulation results

Figure 2 presents the two- and (2+3)-body GEMC results, where the top and bottom panels contain the vapor-liquid coexistence curves and Clausius-Clapeyron plots, respectively. Subcritical simulation results and critical constants are plotted as open and closed symbols, respectively, while Eqs. 4, 5, and 6 are included as lines. For comparison, the (2+3)-body

virial critical constants for $n \to \infty$ are also depicted in Figure 2. Excellent agreement is observed between GEMC and virial critical constant values. Critical constant values obtained with Eqs. 4, 5, and 6 are reported in Table 3, while Table 4 provides tabulated GEMC subcritical coexistence densities, vapor pressures, and vapor compressibility factors.

Table 3: GEMC critical constants. Two-body and (2+3)-body results for $N = 1400$ were obtained with $r_{\text{cut}} = 1.4$ nm and $r_{\text{cut}} = 1.0$ nm, respectively. Expanded uncertainties (95% confidence intervals) are obtained with bootstrap resampling.

Potential	T_{c} (K)	ρ_{c} (mol·L^{-1})	P_{c} (MPa)	Z_{c}
Two-body	13.12(10)	28.6(2)	0.94(4)	0.300(12)
(2+3)-body	13.01(9)	28.6(3)	0.93(4)	0.300(11)

Table 4: GEMC saturation densities, pressure, and vapor compressibility factor. Two-body and (2+3)-body results for $N = 1400$ were obtained with $r_{\text{cut}} = 1.4$ nm and $r_{\text{cut}} = 1.0$ nm, respectively. Expanded uncertainties (95% confidence intervals) are calculated from four independent replicate simulations.

T^{sat} (K)	$\rho_{\text{liq}}^{\text{sat}}$ (mol·L^{-1})	$\rho_{\text{vap}}^{\text{sat}}$ (mol·L^{-1})	P^{sat} (MPa)	$Z_{\text{vap}}^{\text{sat}}$
Two-body				
9	68.51(2)	1.222(9)	0.0832(5)	0.909(2)
9.5	66.37(1)	1.816(7)	0.1263(4)	0.881(1)
10	64.03(5)	2.55(3)	0.180(2)	0.848(3)
10.5	61.51(2)	3.550(10)	0.2502(4)	0.808(2)
11	58.73(4)	4.83(2)	0.336(1)	0.761(5)
11.5	55.56(2)	6.53(2)	0.443(1)	0.711(1)
12	51.93(3)	8.88(4)	0.573(2)	0.648(3)
12.5	46.91(9)	12.15(8)	0.720(3)	0.570(4)
(2+3)-body				
9.0	68.76(5)	1.29(2)	0.0874(14)	0.907(2)
9.5	66.409(10)	1.844(7)	0.1277(4)	0.8789(10)
10.0	64.00(4)	2.66(1)	0.1861(4)	0.841(2)
10.5	61.28(4)	3.66(5)	0.256(3)	0.801(2)
11.0	58.41(5)	5.06(2)	0.348(2)	0.7524(10)
11.5	55.10(5)	6.90(3)	0.460(2)	0.697(2)
12.0	51.16(8)	9.43(10)	0.592(5)	0.629(2)
12.5	45.7(2)	13.08(11)	0.747(3)	0.550(3)

The somewhat large uncertainties in T_{c} and, by consequence, P_{c} are due primarily to the

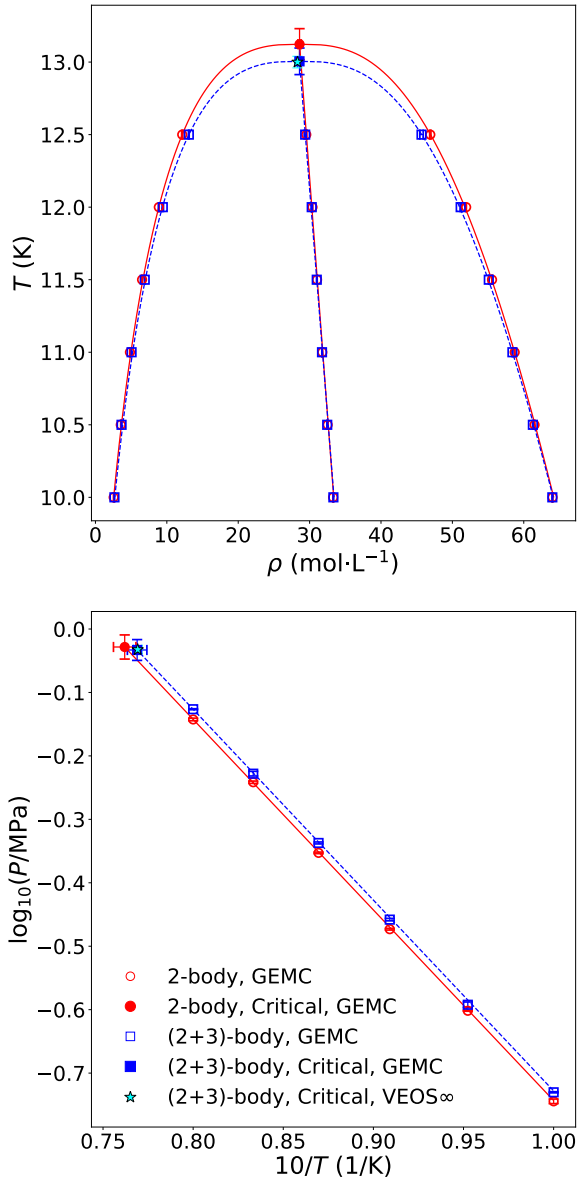

Figure 2: GEMC results for two- and (2+3)-body simulations compared with (2+3)-body virial-extrapolated (VEOS∞) critical constants. Top and bottom panels contain vapor-liquid coexistence curves and Clausius-Clapeyron plots, respectively. Lines represent optimal fits using Eqs. 4, 5, and 6. Open and filled symbols correspond to subcritical GEMC simulation values and critical constants, respectively. Two-body (red circles, solid line) and (2+3)-body (blue squares, dashed line) results for $N = 1400$ were obtained with $r_{\text{cut}} = 1.4$ nm and $r_{\text{cut}} = 1.0$ nm, respectively. Error bars represent 95% confidence intervals and are typically less than one symbol size.

wide range of β values (0.325 to 0.385) considered in Eq. 5 and the high sensitivity of T_{c} to β. Therefore, the uncertainties in the critical constants would not diminish significantly

by including additional state points, increasing the number of replicates, performing longer simulations, or simulating larger systems. However, we believe that considering a wide range of β values is important to capture the extrapolatory uncertainty of the fitting process, whereas assuming a fixed β value would greatly underestimate the "true" uncertainty in the critical constants.

The two- and (2+3)-body vapor-liquid $\rho_{\text{liq}}^{\text{sat}}$ values are nearly indistinguishable at low temperatures ($T_{\text{r}} < 0.95$). By contrast, a noticeable shift exists between the two- and (2+3)-body P^{sat} values. Because three-body forces are not included in the pressure calculation, the larger P^{sat} values for the (2+3)-body case are a direct result of the increase in $\rho_{\text{vap}}^{\text{sat}}$ and, for this reason, the vapor-phase compressibility factor ($Z_{\text{vap}}^{\text{sat}} \equiv \frac{P^{\text{sat}}}{\rho_{\text{vap}}^{\text{sat}} R T^{\text{sat}}}$) is equivalent for the two- and (2+3)-body results. Although the critical constants for the two- and (2+3)-body cases agree within their combined uncertainties, this is again because we have investigated a large range of β values. By contrast, for a fixed value of β, the (2+3)-body T_{c} value is approximately 0.1 K less than the two-body T_{c} value.

Our investigation of finite-size effects demonstrates that the GEMC simulation results are indistinguishable between the 800, 1400, and 2800 molecule systems and the 1.0, 1.4, and 1.8 nm cut-off distances (see Supporting Information). These findings are consistent with those of Reference 14, where they concluded that finite-size effects were negligible for GEMC simulations with between 800 and 5500 Lennard-Jones particles and for cut-off distances between 3.5σ and 8σ. Recall that a 1.0 nm cut-off is approximately equal to 4σ and that the helium two-body potential decays to zero more rapidly than the Lennard-Jones potential. Therefore, it is not surprising that we do not observe significant finite-size effects.

In a further attempt to validate the quality of our subcritical GEMC $\rho_{\text{vap}}^{\text{sat}}$ and P^{sat} values, we confirm that $Z_{\text{vap}}^{\text{sat}}$ follows a physically realistic trend and converges to 1 at low temperatures (see Supporting Information).[52]

Discussion and Conclusions

We have used the highly accurate information available on the intermolecular forces of helium to estimate the critical point of a hypothetical "classical" helium in which quantum effects are absent. The resulting vapor-pressure curve and critical point are shifted dramatically from those of real helium (which has a critical temperature near 5.2 K and a critical pressure near 0.23 MPa),[53] as illustrated in Fig. 3.

Three relatively simple approaches for classical helium, based only on the pair potential, yield critical temperatures between 12.75 K and 13.05 K, with critical pressures between 0.91 MPa and 1.08 MPa. These values are in surprisingly good agreement with our more rigorous results.

Based on two- plus three-body potentials, we estimated the critical point from a virial expansion (calculated to seventh order and extrapolated to infinite order) and from GEMC simulation. Both results are in excellent agreement, producing a critical temperature of 13.0 K, a critical pressure of 0.93 MPa, and a critical density of 28.4 mol·L^{-1}, with 95% confidence intervals on the order of 0.1 K for T_c, 0.02 MPa for P_c, and 0.5 mol·L^{-1} for ρ_c. The effect of three-body interactions is small; they lower the critical temperature by approximately 0.1 K compared to calculations that use only two-body interactions. This strongly suggests that we are justified in ignoring four-body and higher interactions.

Our results indicate that the true critical temperature and pressure of "classical" helium are somewhat larger than the values proposed by Rowland et al.[4] This may be because Rowland et al. optimized their effective critical parameters based on experimental data for helium with methane below 190 K; at these temperatures quantum effects on helium would not be insignificant. Our classical results might be thought of as a high-temperature limit and therefore as upper bounds for the effective T_c and P_c in any given situation, although for process temperatures of 300 K or above the quantum effects should be small.

In principle, our GEMC results could be improved by more detailed simulations and analysis in the critical region, such as that in Ref. 14. Alternatively, more sophisticated

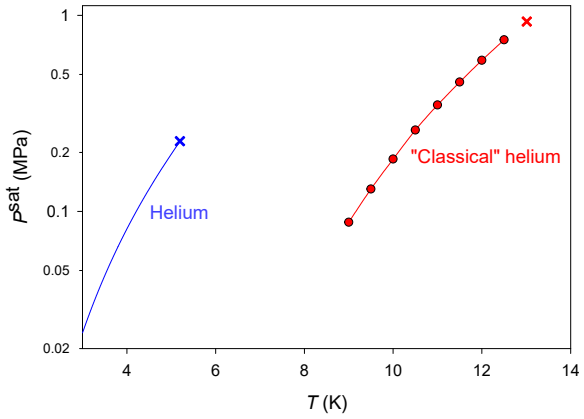

Figure 3: Comparison of vapor-pressure curves for real helium (calculated from the reference equation of state of Ortiz-Vega et al.[53]) and classical helium (from the GEMC results in this work). Critical points are marked with $\times$.

approaches designed specifically to explore the critical region, such as finite-size scaling,[54] could be used. These methods would, however, be quite expensive for the computationally complex potentials used in this study, and our uncertainties are already small enough for our purpose of providing effective classical values for engineering use. Further, the adequacy of our approach is supported by the good agreement with the critical properties given by the VEOS.

The same approach could be applied to other fluids for which quantum effects are significant at the critical temperature. For neon, two-body[55] and three-body[11] potentials exist that, while not of the exquisite accuracy of their helium counterparts, would probably be adequate for these purposes. However, Gunn et al.[2] estimated the critical temperature for classical neon to be 45.5 K, compared to the true critical temperature of 44.4 K, such a small difference that molecular estimation of the classical critical parameters is probably not justified (especially given the limited engineering applications of mixtures with neon). A better candidate would be molecular hydrogen, with its strong quantum effects (half the mass of helium) and a critical temperature near 33 K. A high-accuracy pair potential exists,[56] but Garberoglio[57] found that the existing three-body potentials for H_2 were insufficiently

accurate for quantitative calculations of the third virial coefficient. Because of the many applications of hydrogen, knowledge of its effective classical critical point would be useful, but it appears this must wait until a better three-body potential is developed.

Acknowledgement

We are grateful to Eliseo Marin-Rimoldi of the Molecular Sciences Software Institute for invaluable support in modifying the Cassandra code, and to Alta Fang of NIST for a careful reading of the manuscript. Support for University at Buffalo authors is provided by the U.S. National Institute of Standards and Technology, Award # 70NANB17H334, and by the U.S. National Science Foundation, Grant CBET-1510017. This research was performed while Richard A. Messerly held a National Research Council (NRC) Postdoctoral Research Associateship at NIST.

Supporting Information Available

Results of virial coefficients we calculated in this work are tabulated in a separate supplementary file. This information is available free of charge via the Internet at http://pubs.acs.org/.

Supporting information contains plots for finite-size effects of GEMC simulations, the vapor-phase compressibility factor trend, validation for neglecting three-body forces in the GEMC pressure calculation, and a comparison of Cassandra and Towhee GEMC results.

Literature Cited

(1) Newton, R. H. Activity Coefficients of Gases. *Ind. Eng. Chem.* **1935**, *27*, 302–306.

(2) Gunn, R. D.; Chueh, P. L.; Prausnitz, J. M. Prediction of thermodynamic properties of dense gas mixtures containing one or more of the quantum gases. *AIChE J.* **1966**, *12*, 937–941.

(3) Chueh, P. L.; Prausnitz, J. M. Vapor-Liquid Equilibria at High Pressures. Vapor-Phase Fugacity Coefficients in Nonpolar and Quantum-Gas Mixtures. *Ind. Eng. Chem. Fundam.* **1967**, *6*, 492–498.

(4) Rowland, D.; Hughes, T. J.; May, E. F. Effective Critical Constants for Helium for Use in Equations of State for Natural Gas Mixtures. *J. Chem. Eng. Data* **2017**, *62*, 2799–2811.

(5) Kunz, O.; Wagner, W. The GERG-2008 Wide-Range Equation of State for Natural Gases and Other Mixtures: An Expansion of GERG-2004. *J. Chem. Eng. Data* **2012**, *57*, 3032–3091.

(6) Przybytek, M.; Cencek, W.; Jeziorski, B.; Szalewicz, K. Pair Potential with Submillikelvin Uncertainties and Nonadiabatic Treatment of the Halo State of the Helium Dimer. *Phys. Rev. Lett.* **2017**, *119*, 123401.

(7) Cencek, W.; Patkowski, K.; Szalewicz, K. Full-configuration-interaction calculation of three-body nonadditive contribution to helium interaction potential. *J. Chem. Phys.* **2009**, *131*, 064105.

(8) Przybytek, M.; Cencek, W.; Komasa, J.; Lach, G.; Jeziorski, B.; Szalewicz, K. Relativistic and Quantum Electrodynamics Effects in the Helium Pair Potential. *Phys. Rev. Lett.* **2010**, *104*, 183003.

(9) Cencek, W.; Przybytek, M.; Komasa, J.; Mehl, J. B.; Jeziorski, B.; Szalewicz, K. Effects of adiabatic, relativistic, and quantum electrodynamics interactions on the pair potential and thermophysical properties of helium. *J. Chem. Phys.* **2012**, *136*, 224303.

(10) Schwerdtfeger, P.; Steenbergen, K. G.; Pahl, E. Relativistic coupled-cluster and density-functional studies of argon at high pressure. *Phys. Rev. B* **2017**, *95*, 214116.

(11) Schwerdtfeger, P.; Hermann, A. Equation of state for solid neon from quantum theory. *Phys. Rev. B* **2009**, *80*, 064106.

(12) Garberoglio, G.; Harvey, A. H. First-Principles Calculation of the Third Virial Coefficient of Helium. *J. Res. Nat. Inst. Stand. Technol.* **2009**, *114*, 249–262.

(13) Messerly, R. A.; Knotts, T. A.; Wilding, W. V. Uncertainty quantification and propagation of errors of the Lennard-Jones 12-6 parameters for n-alkanes. *J. Chem. Phys.* **2017**, *146*, 194110.

(14) Dinpajooh, M.; Bai, P.; Allan, D. A.; Siepmann, J. I. Accurate and precise determination of critical properties from Gibbs ensemble Monte Carlo simulations. *J. Chem. Phys.* **2015**, *143*, 114113.

(15) Weaver, A. B.; Alexeenko, A. A. Revised Variable Soft Sphere and Lennard-Jones Model Parameters for Eight Common Gases up to 2200 K. *J. Phys. Chem. Ref. Data* **2015**, *44*, 023103.

(16) Tsonopoulos, C. An empirical correlation of second virial coefficients. *AIChE J.* **1974**, *20*, 263–272.

(17) Song, Y.; Mason, E. A. Equation of state for "classical" helium. *Phys. Rev. E* **1993**, *47*, 2193–2196.

(18) Song, Y.; Mason, E. A. Statistical-mechanical theory of a new analytical equation of state. *J. Chem. Phys.* **1989**, *91*, 7840–7853.

(19) Aziz, R. A.; Slaman, M. J. An examination of ab initio results for the helium potential energy curve. *J. Chem. Phys.* **1991**, *94*, 8047–8053.

(20) Hansen, J.-P.; McDonald, I. *Theory of Simple Liquids*, 4th ed.; Academic Press, London, 2013.

(21) Wheatley, R. J. Calculation of High-Order Virial Coefficients with Applications to Hard and Soft Spheres. *Phys. Rev. Lett.* **2013**, *110*, 200601.

(22) Wheatley, R. J.; Schultz, A. J.; Do, H.; Gokul, N.; Kofke, D. A. A framework for cluster integrals compatible with realistic molecular models. (in preparation).

(23) Shaul, K. R. S.; Schultz, A. J.; Kofke, D. A.; Moldover, M. R. Semiclassical fifth virial coefficients for improved ab initio helium-4 standards. *Chem. Phys. Lett.* **2012**, *531*, 11–17.

(24) Garberoglio, G.; Harvey, A. H. Path-integral calculation of the third virial coefficient of quantum gases at low temperatures. *J. Chem. Phys.* **2011**, *134*, 134106.

(25) Shaul, K. R. S.; Schultz, A. J.; Kofke, D. A. Path-integral Mayer-sampling calculations of the quantum Boltzmann contribution to virial coefficients of helium-4. *J. Chem. Phys.* **2012**, *137*, 184101.

(26) Schultz, A. J.; Kofke, D. A. Virial coefficients of helium-4 from *ab initio*-based molecular models. *J. Chem. Eng. Data* **2019**, (in press).

(27) Singh, J. K.; Kofke, D. A. Mayer sampling: Calculation of cluster integrals using free-energy perturbation methods. *Phys. Rev. Lett.* **2004**, *92*, 220601.

(28) Benjamin, K. M.; Schultz, A. J.; Kofke, D. A. Gas-phase molecular clustering of TIP4P and SPC/E water models from higher-order virial coefficients. *Ind. Eng. Chem. Res.* **2006**, *45*, 5566–5573.

(29) Benjamin, K. M.; Singh, J. K.; Schultz, A. J.; Kofke, D. A. Higher-order virial coefficients of water models. *J. Phys. Chem. B* **2007**, *111*, 11463–11473.

(30) Schultz, A. J.; Kofke, D. A. Quantifying Computational Effort Required for Stochastic Averages. *J. Chem. Theory Comput.* **2014**, *10*, 5229–5234.

(31) Barlow, N. S.; Schultz, A. J.; Kofke, D. A.; Weinstein, S. J. Critical Isotherms from Virial Series Using Asymptotically Consistent Approximants. *AIChE J.* **2014**, *60*, 3336–3349.

(32) Schultz, A. J.; Kofke, D. A. Sixth, seventh and eighth virial coefficients of the Lennard-Jones model. *Mol. Phys.* **2009**, *107*, 2309–2318.

(33) Pelissetto, A.; Vicari, E. Critical phenomena and renormalization-group theory. *Phys. Rep.* **2002**, *368*, 549–727.

(34) Behnejad, H.; Sengers, J. V.; Anisimov, M. A. In *Applied Thermodynamics of Fluids*; Goodwin, A. R. H., Sengers, J. V., Peters, C. J., Eds.; Royal Society of Chemistry, 2010; Chapter 10, pp 321–367.

(35) Barlow, N. S.; Schultz, A. J.; Weinstein, S. J.; Kofke, D. A. Communication: Analytic continuation of the virial series through the critical point using parametric approximants. *J. Chem. Phys.* **2015**, *143*, 071103.

(36) Schultz, A. J.; Barlow, N. S.; Chaudhary, V.; Kofke, D. A. Mayer Sampling Monte Carlo calculation of virial coefficients on graphics processors. *Mol. Phys.* **2013**, *111*, 535–543.

(37) Feng, C.; Schultz, A. J.; Chaudhary, V.; Kofke, D. A. Eighth to sixteenth virial coefficients of the Lennard-Jones model. *J. Chem. Phys.* **2015**, *143*, 044504.

(38) Pérez-Pellitero, J.; Ungerer, P.; Orkoulas, G.; Mackie, A. Critical point estimation of the Lennard-Jones pure fluid and binary mixtures. *J. Chem. Phys.* **2006**, *125*, 054515.

(39) Potoff, J. J.; Panagiotopoulos, A. Z. Critical point and phase behavior of the pure fluid and a Lennard-Jones mixture. *J. Chem. Phys.* **1998**, *109*, 10914–10920.

(40) Panagiotopoulos, A. Z. Monte Carlo methods for phase equilibria of fluids. *J. Phys.: Cond. Matter* **2000**, *12*, R25–R52.

(41) Shah, J. K.; Marin-Rimoldi, E.; Mullen, R. G.; Keene, B. P.; Khan, S.; Paluch, A. S.; Rai, N.; Romanielo, L. L.; Rosch, T. W.; Yoo, B.; Maginn, E. J. Cassandra: An open source Monte Carlo package for molecular simulation. *J. Comput. Chem.* **2017**, *38*, 1727–1739.

(42) Morales, A. D. C.; Economou, I. G.; Peters, C. J.; Siepmann, J. I. Influence of simulation protocols on the efficiency of Gibbs ensemble Monte Carlo simulations. *Molecular Simulation* **2013**, *39*, 1135–1142.

(43) Sadus, R. J.; Prausnitz, J. M. Three-body interactions in fluids from molecular simulation: Vapor-liquid phase coexistence of argon. *J. Chem. Phys.* **1996**, *104*, 4784–4787.

(44) Marcelli, G.; Sadus, R. J. Molecular simulation of the phase behavior of noble gases using accurate two-body and three-body intermolecular potentials. *J. Chem. Phys.* **1999**, *111*, 1533–1540.

(45) Martin, M. G. MCCCS Towhee. http://towhee.sourceforge.net/. `http://towhee.sourceforge.net/`.

(46) L'Ecuyer, P. Tables of Maximally Equidistributed Combined LFSR Generators. *Math. Comput.* **1999**, *68*, 261–269.

(47) Deng, L.-Y. Efficient and Portable Multiple Recursive Generators of Large Order. *ACM Trans. Model. Comput. Simul.* **2005**, *15*, 1–13.

(48) Rowlinson, J. S.; Swinton, F. *Liquids and liquid mixtures: Butterworths monographs in chemistry*; Butterworth-Heinemann, 2013.

(49) Rowlinson, J. S.; Widom, B. *Molecular theory of capillarity*; Courier Corporation, 2013.

(50) Levelt Sengers, J. M. H.; Greer, W. L.; Sengers, J. V. Scaled Equation of State Parameters for Gases in the Critical Region. *J. Phys. Chem. Ref. Data* **1976**, *5*, 1–51.

(51) Messerly, R. A.; Rowley, R. L.; Knotts, T. A.; Wilding, W. V. An improved statistical analysis for predicting the critical temperature and critical density with Gibbs ensemble Monte Carlo simulation. *J. Chem. Phys.* **2015**, *143*, 104101.

(52) Nezbeda, I. Simulations of vapor-liquid equilibria: Routine versus thoroughness. *J. Chem. Eng. Data* **2016**, *61*, 3964–3969.

(53) Ortiz-Vega, D. O.; Hall, K. R.; Holste, J. C.; Arp, V. D.; Harvey, A. H.; Lemmon, E. W. Reference Equation of State for Helium-4. *J. Phys. Chem. Ref. Data* **2019**, (in preparation).

(54) Wilding, N. B. Simulation studies of fluid critical behavior. *J. Phys. Cond. Matter* **1997**, *9*, 585–612.

(55) Hellmann, R.; Bich, E.; Vogel, E. Ab initio potential energy curve for the neon atom pair and thermophyiscal properties of the dilute neon gas. I. Neon-neon interatomic potential and rovibrational spectra. *Mol. Phys.* **2008**, *106*, 133–140.

(56) Garberoglio, G.; Jankowski, P.; Szalewicz, K.; Harvey, A. H. Second virial coefficients of H_2 and its isotopologues from a six-dimensional potential. *J. Chem. Phys.* **2012**, *137*, 154308.

(57) Garberoglio, G. On the contribution of non-additive three-body interactions to the third virial coefficient of *para*-hydrogen. *Chem. Phys. Lett.* **2013**, *557*, 26–30.

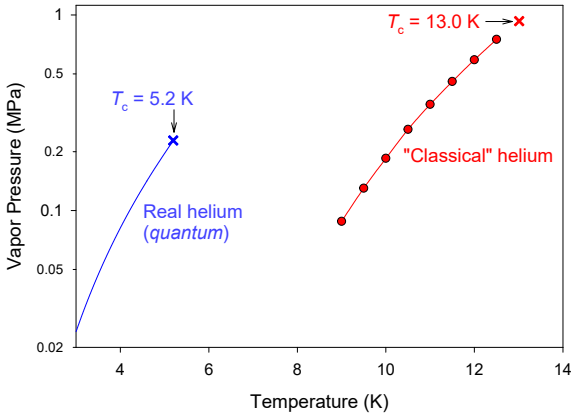

Figure 4: for Table of Contents use only. Molecular Calculation of the Critical Parameters of Classical Helium: Richard A. Messerly, Navneeth Gokul, Andrew J. Schultz, David A. Kofke, and Allan H. Harvey